nature water

Article

https://doi.org/10.1038/s44221-023-00070-z

Removal of pharmaceutical pollutants from effluent by a plant-based metal–organic framework

Received: 1 July 2022

Accepted: 16 March 2023

Published online: 15 May 2023

Check for updates

Erik Svensson Grape[1], Antonio J. Chacón-García[2], Sara Rojas[2], Yolanda Pérez[2,3], Aleksander Jaworski[1], Mathias Nero[1], Michelle Åhlén[4], Eva Martínez-Ahumada[5], Athina E. Galetsa Feindt[1], Mathieu Pepillo[1,6], Mayumi Narongin-Fujikawa[7], Ilich A. Ibarra[5], Ocean Cheung[4], Christian Baresel[7], Tom Willhammar[1] ✉, Patricia Horcajada[2] ✉ & A. Ken Inge[1] ✉

Emerging organic contaminants (EOCs), such as pharmaceutical compounds, are of growing environmental concern, and there is a need to develop new materials and technologies for their efficient removal. Here we developed a highly porous and stable zirconium–ellagate framework, denoted SU-102, which was used to remove EOCs from water, including real municipal wastewater treatment plant effluent. SU-102 adsorbs cationic EOCs with particularly high efficiencies, and of the 17 pharmaceutical EOCs detected in wastewater treatment plant effluent, all 9 cationic species were removed with efficiencies of at least 79.0–99.6%, emphasizing the importance of framework charge on selectivity. As a second mechanism of EOC removal, SU-102 photodegraded the antibiotic sulphamethazine under visible light. SU-102 is synthesized from ellagic acid, an edible polyphenol building unit, highlighting the possibility of creating stable high-performance multi-functional materials from sustainably sourced plant-based components.

Ensuring the availability of freshwater is a fundamental challenge on a global scale, with 80% of the world's population being at risk of water scarcity or insecurity[1]. In addition, water plays an essential role in ecosystem balance and the continued preservation of biodiversity across our planet[2]. While many pollutants are removed in conventional wastewater treatment plants (WWTPs), sequestration of emerging organic contaminants (EOCs) has proved challenging[3,4]. EOCs include pharmaceuticals and personal care products, dyes, pesticides, and veterinary and industrial products[4], and their presence at concentrations on the order of micrograms to nanograms per litre can have negative effects on living organisms[5]. Recent studies revealed that environmentally concerning concentrations of pharmaceutical pollutants were found in more than a quarter of 1,052 locations tested across 104 countries[6]. These observations, coupled with low removal rates (<50%) of many currently implemented WWTP technologies, have directed interest towards alternative removal methods, including the use of adsorbents[5].

[1]Department of Materials and Environmental Chemistry, Stockholm University, Stockholm, Sweden. [2]Advanced Porous Materials Unit, IMDEA Energy, Madrid, Spain. [3]Departamento de Biología y Geología, Física y Química Inorgánica, ESCET, Universidad Rey Juan Carlos, Madrid, Spain. [4]Division of Nanotechnology and Functional Materials, Department of Materials Science and Engineering, Ångström Laboratory, Uppsala University, Uppsala, Sweden. [5]Laboratorio de Fisicoquímica y Reactividad de Superficies (LaFReS), Instituto de Investigaciones en Materiales, Universidad Nacional Autónoma de México, Mexico City, Mexico. [6]Départment Sciences et Génie Des Matériaux, INSA, Lyon, France. [7]IVL Swedish Environmental Research Institute, Stockholm, Sweden. ✉e-mail: tom.willhammar@mmk.su.se; patricia.horcajada@imdea.org; andrew.inge@mmk.su.se

An ideal EOC adsorbent should possess a high degree of porosity to maximize interactions with EOCs even when present at very low concentrations, demonstrate good stability under working conditions, be made of environmentally friendly components and have a low production cost. However, commonly used amorphous adsorbents, such as activated carbon, come with the inherent drawback of ill-defined structures and often limited removal efficiencies (REs). Crystalline porous materials, such as metal–organic frameworks (MOFs), offer high surface areas as well as well-defined pore dimensions and chemical environments, which can form favourable interactions between the framework and targeted adsorbates.

Comprising metal ions and organic linker molecules, MOFs provide a wide variety of host–guest interactions, thereby promoting selective separation of pollutants while also providing catalytically active sites capable of degrading contaminants. While MOFs show promising results for EOC removal[7], no studies have, to the best of our knowledge, reported their uptake of pharmaceutical compounds from real and unspiked WWTP effluent, where EOCs are found as a complex cocktail of contaminants[5].

In this article, we developed a robust MOF with the aim of attaining an efficient water remediation agent made of building blocks that are non-toxic and sustainably sourced when possible. For the organic part of the MOF, we turned to ellagic acid (Fig. 1a), an abundant phytochemical that is isolated from plant material such as tree bark and fruit peels—materials that are otherwise considered as waste from the food, pulp and paper industries[8]. Ellagic acid is a building unit of tannins, a class of naturally occurring polyphenolic biomolecules that are the second largest source of natural aromatic molecules, following lignin[9]. As a common antioxidant, it is sold commercially as a dietary supplement, making it considerably cheaper compared with many MOF linkers of similar size.

We recently reported the first MOF made with ellagic acid[10], which was synthesized from biocompatible components and under green synthesis conditions. However, with a pore diameter of 7 Å, investigations were limited to the capture of small molecules or ions[11]. Following this, we aimed to develop other stable and biocompatible metal–ellagate frameworks with wider pores to facilitate capture of larger molecules.

To promote stability in MOFs, high-valence metal cations are often combined with organic linkers bearing carboxylate groups. As such, Zr(IV) cations have been of particular interest for the synthesis of MOFs[12]. In recent years, combining Zr(IV) with phenol-bearing organic ligands has yielded a handful of MOFs, all with remarkable chemical stabilities, yet they have been made from non-commercial synthetic ligands[13–16].

Here, we present a zirconium–ellagate framework, denoted SU-102, created with the aim of combining the high chemical stability of Zr-MOFs with the renewable sourcing, biocompatibility and relatively low cost of a commercially available plant-based organic linker. SU-102 efficiently removes many challenging EOCs from water, demonstrated using real WWTP effluent. Laboratory-scale tests with select pharmaceutical compounds at higher concentrations indicate that SU-102 simultaneously acts as both an adsorbent and a photocatalyst of EOCs.

Synthesis, structure and characterization of SU-102

SU-102 was first synthesized under solvothermal conditions in a mixture of water, acetic acid and *N*,*N*-dimethylformamide (DMF), from zirconyl chloride and ellagic acid. SU-102 can be synthesized using either chemical grade (95% purity) or dietary supplement grade (90% purity) ellagic acid. DMF can be substituted for *N*,*N*-diethylformamide, or an aqueous solution of either dimethylamine or ammonia. In contrast to other Zr–phenolate MOFs that were synthesized over 24 h or longer[13–16], the synthesis of SU-102 takes only 1 h (84% yield after activation). SU-102 can also be synthesized at ambient pressure (Supplementary Fig. 1), making it possible to scale up the synthesis to the multi-gram scale. Crystallinity and phase purity were confirmed by powder X-ray diffraction (PXRD) (Supplementary Figs. 2 and 3 and Supplementary Table 1) as well as scanning electron microscopy (Supplementary Fig. 4), which showed an average particle length of 0.98 ± 0.66 µm and a width of 0.19 ± 0.06 µm (measured from 300 particles).

The structure of as-synthesized SU-102 was solved and refined (Supplementary Fig. 5 and Supplementary Table 2) using three-dimensional (3D) electron diffraction (ED), also known as microED, which allows for the collection of single-crystal diffraction data from submicrometre-sized crystals[17]. SU-102 crystallizes in the rhombohedral space group $R\bar{3}c$ and has a honeycomb arrangement of 1D channels (Fig. 1b) with an accessible diameter of 12 Å. The Zr(IV) cations are found in isolated ZrO_8 units with square anti-prism coordination geometry (Fig. 1d). Each Zr(IV) cation is chelated by catecholate groups of four ellagate anions, resulting in a 3D framework that can be described by the **pts** net[18].

Remarkably, all hydrogen atoms of the framework could be located from the 3D ED data[19]. The ellagate anions remain partially protonated, with one phenol hydrogen per ellagate bridging the ZrO_8 units by hydrogen bonds in a helical arrangement along the *c* axis (Fig. 1d). Additionally, the framework is supported through π–π stacking of ellagate anions along the *c* direction, with carbonyl groups protruding into the channels.

The structure was further validated by scanning transmission electron microscopy (STEM) using both annular dark-field (ADF) and integrated differential phase contrast (iDPC) signals (Fig. 1e–g). ADF imaging, which emphasizes heavier elements, clearly highlighted the positions of Zr(IV) cations in the crystals, while iDPC imaging provides more contrast to lighter atoms such as carbon and oxygen, accentuating the ellagate anions (see Supplementary Fig. 6 for the raw images). Both imaging techniques indicated a high degree of order in the crystals of SU-102.

Elemental analysis of SU-102 after activation suggested the presence of charge-balancing dimethylammonium (DMA) cations within the pores, implying an anionic framework. The generation of DMA, a compound naturally found in plants and animals[20], through hydrolysis is a common phenomenon when DMF is used as a solvent in MOF synthesis. Crystal structure refinement against the 3D ED data revealed the location of the DMA cations in the pores, forming hydrogen bonds to phenol and lactone groups of the framework. Furthermore, ^{1}H and ^{13}C magic-angle spinning (MAS) solid-state nuclear magnetic resonance (NMR) indicated the presence of one DMA cation per ellagate anion and that one phenolic group remained protonated on each ellagate anion, which is in good agreement with the 3D ED model and the sum formula of $(C_2H_8N)_2[Zr(C_{14}H_3O_8)_2]\cdot 6H_2O$ (Supplementary Figs. 7 and 8).

To further validate the anionic nature of the framework, ion exchange was performed to replace DMA cations in the pores with Li^+, Na^+ and K^+ (Supplementary Figs. 8–18 and Supplementary Tables 3 and 4). In Na-exchanged SU-102, ^{1}H and ^{13}C MAS solid-state NMR confirmed the absence of DMF in the product and that the DMA cations can be fully exchanged for Na^+ by stirring SU-102 in aqueous NaCl solution (Supplementary Fig. 8). ^{23}Na MAS solid-state NMR showed a distinct environment for the Na^+ cations interacting with the organic linker. Cation exchange had profound effects on gas sorption properties of SU-102: exchanging the counterion from DMA to Na^+ increased the Brunauer–Emmett–Teller (BET) surface area from 472 to 573 $m^2\,g^{-1}$ (Supplementary Figs. 11 and 13), and additional gas sorption measurements indicated that the CO_2 uptake capacity was enhanced by K^+ exchange, increasing from ~27 to ~90 $cm^3\,g^{-1}$ (at 293 K and 1 bar), while the CO_2-over-N_2 selectivity also increased from 12 to 81 (Supplementary Table 4). The enhanced CO_2 uptake may be a result of an increased electric field gradient with respect to the framework[21]. Additionally, CO_2 could also be interacting directly with the cation, with K^+ potentially providing a larger area of interaction sites[22].

https://doi.org/10.1038/s44221-023-00070-z

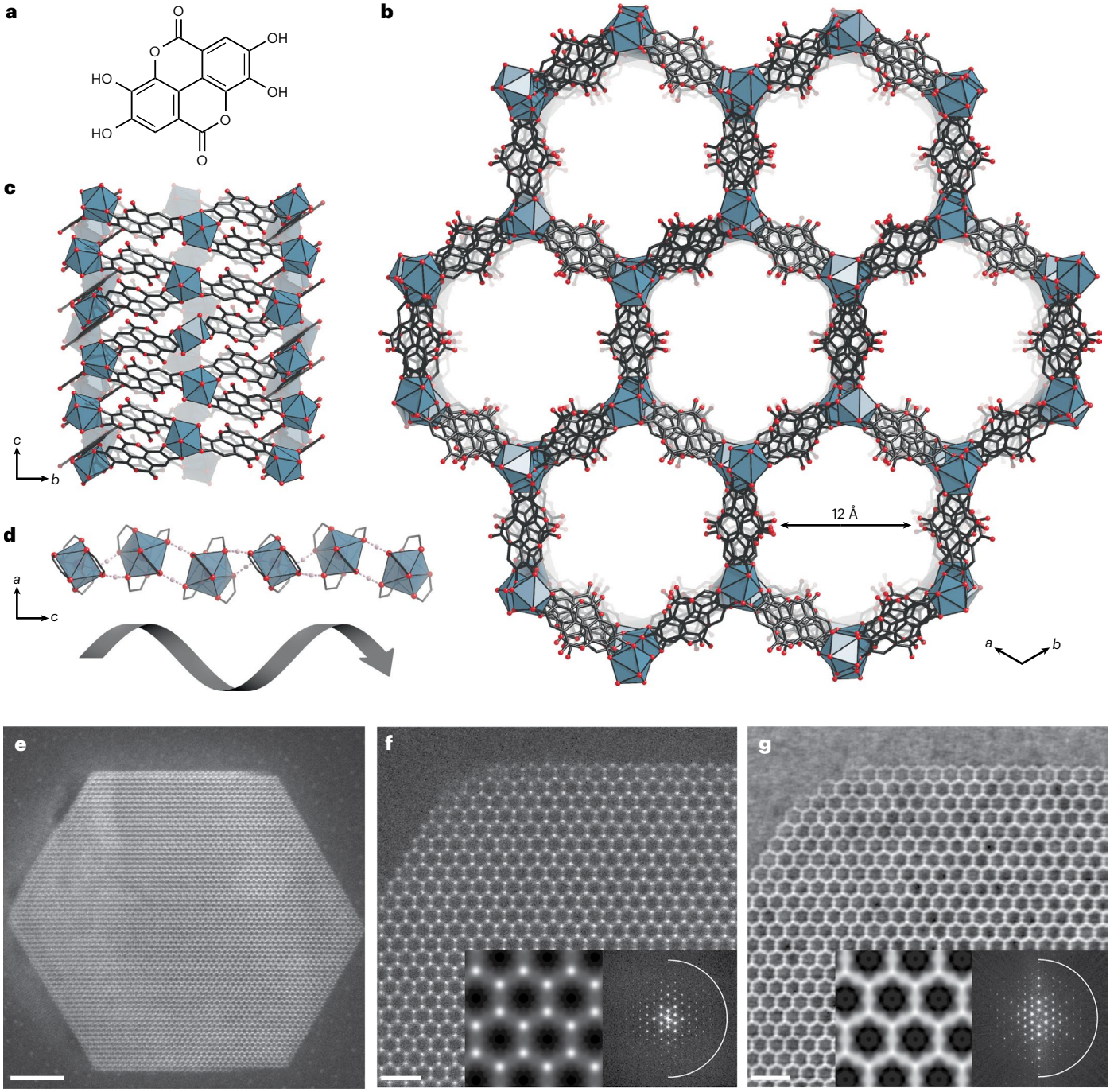

Fig. 1 | Structure of the Zr–ellagate SU-102. a, Molecular structure of ellagic acid. **b**, The crystal structure of SU-102 as viewed down the one-dimensional channels that extend along the *c* axis. Hydrogen atoms and charge-balancing guest species have been omitted for clarity. ZrO_8 units are shown as blue polyhedra. **c**, Side view of a channel wall, as viewed along the *a* axis. **d**, ZrO_8 units stacked along the *c* axis and bridged by pairs of strong hydrogen bonds between phenol and phenolate groups to form helices. O–H bonds are drawn as dashed lines and only phenolate-bonded carbons are shown. **e**, ADF STEM image of a crystal of SU-102 (scale bar, 20 nm). **f**,**g**, STEM images of SU-102 using ADF (**f**) and iDPC (**g**) signals (scale bars, 5 nm). Insets in **f** and **g** show the lattice-averaged maps with *p6mm* symmetry imposed (left) and Fourier transforms (right) of each respective image. The half circles indicate a resolution of 2.5 Å.

As anticipated for a zirconium–phenolate framework, SU-102 demonstrated chemical robustness in various conditions. In aqueous media the MOF was stable according to PXRD in a pH range of 3–12 (Supplementary Fig. 19), in phosphate-buffered saline (>14 days; although with some changes to PXRD intensities, Supplementary Fig. 20), and under hydrothermal conditions (Supplementary Fig. 21), as was also validated through nitrogen adsorption (Supplementary Fig. 22). Comparing the aqueous stability of SU-102 with the five published Zr–phenolate MOFs, SU-102 performs as well as MIL-163 (ref. 13), while exhibiting lower acid/base stability than ZrPP-1 (pore size ~4 Å), yet higher than that of ZrPP-2 (pore size ~8 Å) (ref. 15). Comparing with UiO-67 (ref. 23), a Zr-MOF of similar pore size, the stability of SU-102 in various media is higher, highlighting the possibility of constructing chemically robust and cheaper MOFs with larger pores through the use of phenolate linkers. SU-102 was stable in many organic solvents, although partial degradation occurred in some aprotic solvents at 80 °C (Supplementary Fig. 21). Thermal stability was investigated by PXRD (Supplementary Fig. 23), showing an intact framework up to

300 °C. SU-102 was also stable in the acidic gaseous environment of SO_2, showing a type-I adsorption isotherm and an SO_2 uptake of 2.8 mmol g^{-1} (Supplementary Figs. 24–27 and Supplementary Table 5).

Selective adsorption of EOCs in real WWTP effluent by SU-102

To study the adsorption of EOCs from complex mixtures at practically relevant concentrations, municipal wastewater treated by a membrane bioreactor (MBR), the process currently implemented at the WWTP in Stockholm, was collected for analysis and treatment by SU-102. Analysis of the effluent indicated the presence of 17 different EOCs at concentrations above the limit of quantification (Fig. 2 and Supplementary Tables 6 and 7), ranging from 32 to 1,400 ng l^{-1}. After treatment with SU-102, the concentrations of all 17 EOCs decreased, while the MOF remains intact (Supplementary Fig. 28). After SU-102 treatment, citalopram, atenolol (At), trimethoprim and sertraline had concentrations below the limit of detection (LOD), while tramadol, propranolol, clarithromycin and naproxen were found below the limit of quantification (LOQ) (Supplementary Table 6). REs of >99% were achieved for At, citalopram and trimethoprim, and REs ≥79% were achieved for 10 of the 17 EOCs. It should be noted that, for the EOCs that were below the LOD/LOQ after SU-102 treatment, the REs shown in Fig. 2 were calculated using the values of the LOD/LOQ concentration and are probably underestimated.

Of particular note is the high RE of metoprolol (98%), which showed the second highest concentration before SU-102 treatment (1,100 ng l^{-1}). Also of note is the high RE of the anti-depressant citalopram (>99%), which was ranked in a 2019 report as the highest risk and priority for the Himmerfjärden WWTP[24], followed by oxazepam.

The wide range of observed REs, between 19% and >99%, indicates strong selectivity in adsorbing certain EOCs over others. The adsorption selectivity depends on numerous factors such as pore accessibility (size and geometry) and inter-molecular interactions between the MOF and the EOC (for example, hydrogen bonds, van der Waals forces and electrostatic interactions). In general, all EOCs with acidic carboxylic acid groups (diclofenac, furosemide and naproxen) had lower REs, while all those bearing basic tertiary amine groups (citalopram, clarithromycin, tramadol and venlafaxine) were adsorbed with high REs. Moreover, an inspection of estimated pK_a values of the 17 EOCs (Supplementary Table 7) revealed that the nine pharmaceuticals removed with the highest REs all had pK_a values for the strongest basic group that were higher than the pH of the effluent (pH 6.4). This indicates that those nine EOCs were predominantly in their cationic forms in the effluent, typically through protonation of a secondary or tertiary amine. All eight other EOCs had pK_a values lower than 6.4 and are thus probably present in their neutral or anionic forms. In summary, REs of cationic EOCs were between 79% and 99%, neutral EOCs between 19% and 79%, and anionic EOCs between 19% and 38% (Fig. 2). The observation that all EOCs with an expected net positive charge were removed with high REs indicates that electrostatic interactions play a dominant role in the selectivity of EOCs adsorbed by SU-102. The use of Na-exchanged SU-102 for EOC sequestration under similar conditions was evaluated, showing that the general trend remains (Supplementary Table 8), although the REs of tramadol, oxazepam and carbamazepine are slightly decreased.

To the best of our knowledge, this is the first study utilizing a MOF to remove EOCs from real WWTP effluent without spiking the water with EOCs. The results clearly indicate that SU-102 can efficiently sequester many EOCs that are currently not removed by WWTPs.

Combined adsorption and photodegradation of EOCs by SU-102

To further investigate the removal of EOCs by SU-102, we selected three EOCs commonly encountered at high concentrations in wastewater and often poorly removed by WWTPs[25,26]: the β-blocker At, the veterinary antibiotic sulphamethazine (SMT) and the anti-inflammatory diclofenac (DCF). These persistent EOCs can have severely toxic effects[19], such as renal dysfunction for At and DCF[27,28], as well as hormone imbalance and potential development of bacterial resistance for SMT[29]. For adsorption experiments, SU-102 was suspended in separate tap water solutions spiked with higher concentrations of At (70 mg l^{-1}), SMT (10 mg l^{-1}) or DCF (15 mg l^{-1}), and the adsorption of the contaminants was quantified by high-performance liquid chromatography (HPLC; Methods and Supplementary Figs. 29–32). The selection of EOC concentrations was based on reported data of severely contaminated waters (for example, sulphonamides >1 mg l^{-1}, At >8 mg l^{-1}, DCF ~1 mg l^{-1}) (refs. 30–33), but further concentrated (approximately tenfold) to ensure accurate detection. At these higher concentrations, SU-102 was able to adsorb up to 70%, 19% and 11% of At, SMT and DCF, respectively, within 2 h (Fig. 3).

These three EOCs are predominantly cationic, neutral and anionic, respectively, at the pH of the tap water (pH ~6; Supplementary Table 7), confirming the higher affinity of SU-102 to cationic species and suggesting electrostatic interactions as the main driving force for adsorption. Additionally, the influence of pH on the adsorption of SMT was evaluated (Supplementary Fig. 33). SMT is expected to be protonated at pH 2 and the RE is indeed much higher compared with the results at pH 6.4 (60.8% versus 24.5%, respectively, after 5 h), further confirming the importance of electrostatic interactions for adsorption.

The robustness of SU-102 during water treatment was studied, showing no detectable ligand leaching by HPLC and unaltered PXRD patterns (Fig. 3c). Comparing SU-102 with other MOFs investigated for At, SMT or DCF removal, SU-102 shows a range of better, similar or lower REs, yet after 24 h no degradation of SU-102 was detected (Supplementary Table 9). Compared with other commonly used synthetic linkers, the low cost and biocompatible character of the natural ellagate ligand makes SU-102 highly competitive for long-term use. Further, it was discovered that concentrated sodium chloride solutions could be used to regenerate SU-102 (Supplementary Fig. 34)[34], facilitating complete removal of previously loaded At, and highlighting the potential of reusing the material as an adsorbent.

In view of the previously reported photocatalytic activity of other Zr-based MOFs[35], photodegradation studies of At, SMT and DCF by SU-102 were performed under similar conditions as the adsorption experiments (Fig. 3b and Supplementary Table 9). While At and DCF appear to be removed exclusively by adsorption, SU-102 acted as an efficient photocatalyst in the elimination of SMT (38% for adsorption versus 100% for adsorption and photodegradation). With an estimated band gap of 2.73 eV (Supplementary Fig. 35), SU-102 was able to efficiently degrade SMT under visible light irradiation (>90% after 7 h), while retaining its structural and chemical integrity. Thus, the combination of both sorption and catalytic processes in a single MOF could pave the way to remove a large variety of EOCs from contaminated water. Additionally, reusability of SU-102 for the photodegradation of SMT was confirmed for at least seven successive cycles (Supplementary Figs. 36 and 37).

Intermediates and photodegradation products of SMT were investigated by liquid chromatography–mass spectrometry (LC–MS) (Supplementary Fig. 38). During photodegradation, peaks emerged consistent with the formation of (4,6-dimethylpyrimidin-2-yl)sulphonic amide, 4-aminobenzenesulphinate, maleic acid and phenol[36]. A proposed mechanism for SMT degradation is shown in Supplementary Fig. 39. Quantitative structure–activity relationship calculations indicated that the developmental toxicity of the degradation products are notably lower than SMT (Supplementary Fig. 40).

In addition, the simultaneous degradation of a mixture of three contaminants (At, DCF and SMT) in tap water was also investigated, showing that the RE of At and SMT remains unaffected (Supplementary Fig. 41) in the mixture, while the RE of DCF was doubled (48% versus 24%, 24 h). This could possibly be explained by the presence of reactive species formed during the photodegradation of SMT, as outlined above.

https://doi.org/10.1038/s44221-023-00070-z

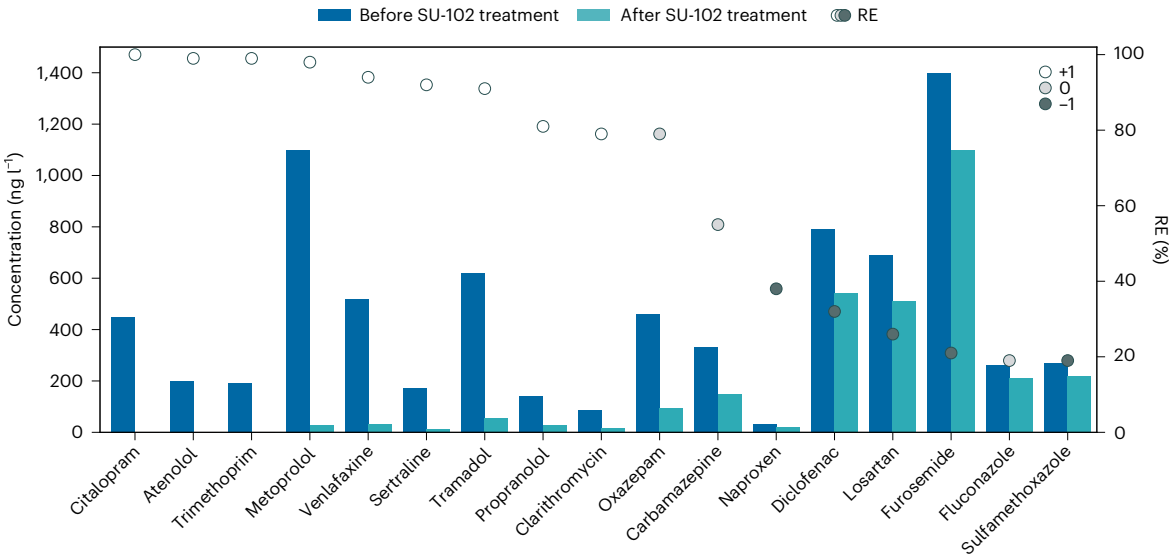

Fig. 2 | Removal of pharmaceutical pollutants from WWTP effluent from IVL Hammarby Sjöstadsverk, Sweden. a, Bars indicate concentrations of pharmaceutical pollutants detected in effluent water before and after SU-102 treatment. Circles indicate the RE of each EOC with colours indicating the expected net charge of the EOC under the studied conditions (pH 6.4). Cationic EOCs (+1) are removed with high efficiency compared with neutral (0) and anionic (−1) EOCs. After SU-102 treatment, the concentrations of eight EOCs were below the LOD or the LOQ. In these cases, the concentration after SU-102 treatment shown is the LOD or LOQ concentration, and thus the actual concentrations after treatment may be lower and the REs may be higher than shown.

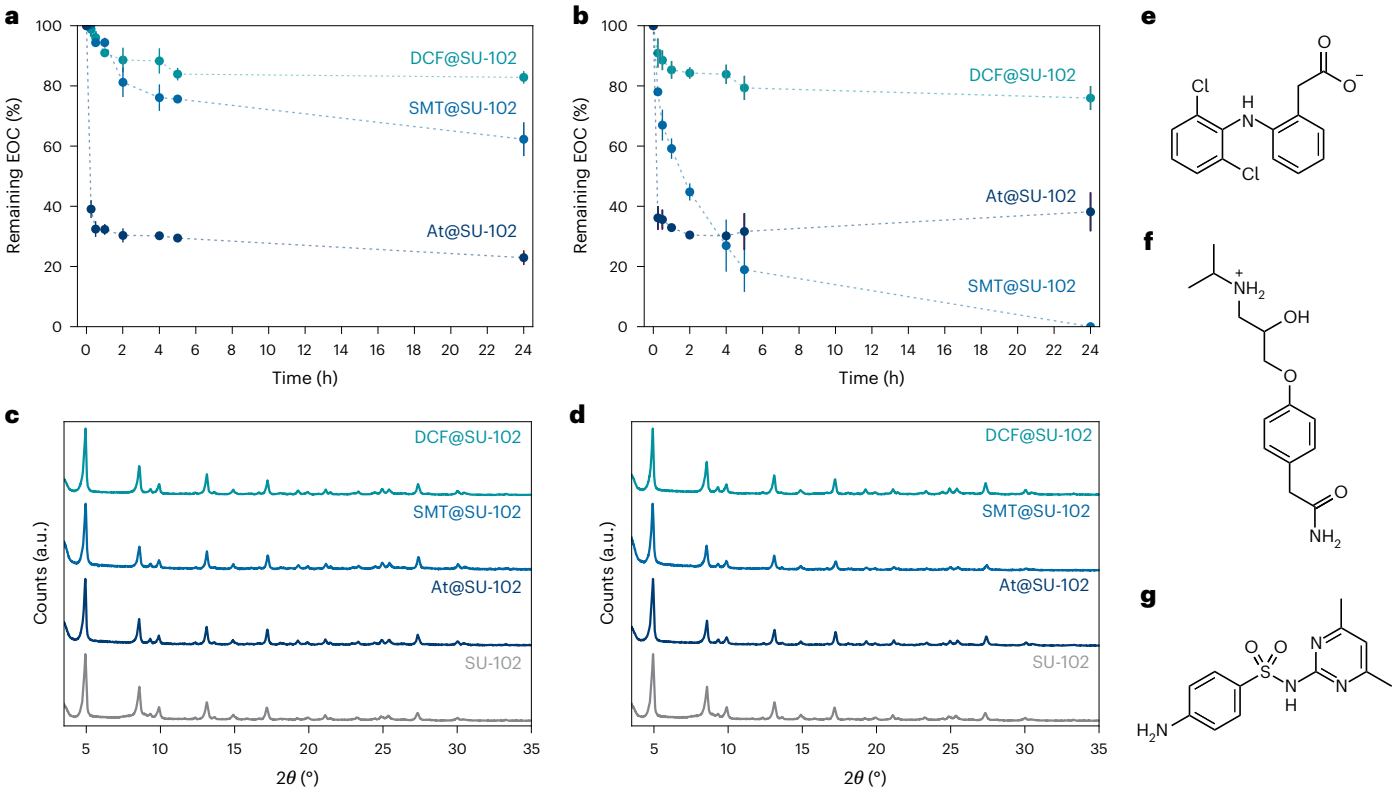

Fig. 3 | Adsorption and photodegradation of selected pharmaceutical pollutants. a,**b**, Comparative removal of At (70 mg l^{-1}), SMT (10 mg l^{-1}) and DCF (15 mg l^{-1}) by adsorption (**a**) and photodegradation (**b**) using SU-102, showing the average value of triplicate experiments with error bars representing 1 s.d. **c**,**d**, PXRD patterns (λ = 1.5406 Å) of SU-102 after being suspended in tap water solutions of At, SMT and DCF while stirring (**c**, for adsorption studies) and under visible light irradiation (**d**, photodegradation assays). **e**–**g**, Molecular structure drawings of DCF (**e**), At (**f**) and SMT (**g**) with their expected charges at pH 6.4.

Conclusions

A chemically robust Zr(IV) MOF made from ellagic acid, a plant-sourced molecule isolated from food waste, was synthesized and its structure unveiled using advanced transmission electron microscopy (TEM) techniques, showing a uniform anionic framework with a well-ordered porous structure. As anticipated for a Zr–phenolate MOF, SU-102

demonstrated exceptional chemical stability, remaining intact over a large pH range and under hydrothermal conditions. To approach practically relevant conditions, the potential of SU-102 to adsorb EOCs from WWTP effluent was investigated, showing a particularly high RE for 10 out of 17 contaminants, which were not fully sequestered using current WWTP processes. Cationic contaminants were preferentially adsorbed by the anionic SU-102, and the relationship between high RE and the expected charge of the EOCs suggests that the selectivity and RE may be adjusted by altering the pH of the water, which could be beneficial for controlling adsorption and desorption. Furthermore, photodegradation was successfully demonstrated on SMT as a second removal mechanism, demonstrating both reusability and better stability compared with other MOFs. The anionic nature of SU-102 also allows for tuning the composition, accessible pore size and properties of the MOF by cation exchange. On the basis of the high affinity of anionic SU-102 for capturing cationic EOCs, it is hypothesized that cationic MOFs may be of interest for the selective capture of anionic EOCs such as DCF. Furthermore, the use of multiple adsorbents made from sustainably sourced building blocks would facilitate highly efficient sequestration of a broad range of pollutants—a crucial aspect of ensuring freshwater availability while maintaining the overarching goal of sustainability.

Methods

Synthesis and physical characterization

SU-102 was initially synthesized by adding 60 mg of ellagic acid (Acros Organics, 97%) and 32 mg of $ZrOCl_2{\cdot}8H_2O$ (Sigma-Aldrich, reagent grade, 98%) into a 5 ml borosilicate 3.3 glass tube (Duran 12 × 100 mm, DWK Life Sciences) containing 2 ml DMF, 1 ml deionized water and 1.5 ml acetic acid. The glass tube was then sealed with a polybutylene terephthalate cap containing a polytetrafluoroethylene (PTFE) seal and heated at 120 °C for 1 h while stirring. The resulting yellow suspension was then centrifuged at 6,000*g* for 10 min and decanted. The remaining solid was then dried overnight at 80 °C. The yield after activation was 65.5 mg, corresponding to 84% of the theoretical yield (78 mg). EOC removal experiments were carried out using SU-102 prepared through this procedure. As the reactions were carried out under hydrothermal conditions, care should be taken when reproducing the synthesis as a high pressure is generated upon heating the reaction vessel.

A ten-fold up-scaled synthesis was carried out under reflux conditions by adding 600 mg of ellagic acid (Acros Organics, 97%) and 320 mg of $ZrOCl_2{\cdot}8H_2O$ (Sigma-Aldrich, reagent grade, 98%) into a 100 ml round-bottom flask containing a mixture of 20 ml DMF, 10 ml deionized water and 15 ml acetic acid. A PTFE stir bar was added and a reflux condenser attached to the flask, which was then heated to 80 °C for 48 h using an oil bath. The contents were then centrifuged at 6,000*g* for 10 min, and the remaining solid was dried at 80 °C overnight. The yield after activation was 0.638 g, corresponding to 82% of the theoretical yield (0.780 g).

SU-102 was also acquired in other solvent mixtures after 1 h at 160 °C (Supplementary Fig. 1) by adding 60 mg ellagic acid (Acros Organics, 97%) and 32 mg $ZrOCl_2{\cdot}8H_2O$ (Sigma-Aldrich, reagent grade, 98%) into a 5 ml borosilicate 3.3 glass tube (Duran 12 × 100 mm, DWK Life Sciences) containing a mixture of 2.5 ml deionized water and 1 ml acetic acid with either 0.1 ml DMF, 0.5 ml *N*,*N*-diethylformamide or 0.1 ml aqueous solutions of dimethylamine (40 wt%) or ammonia (25 wt%).

For stability tests, 10 mg SU-102 was immersed in 1 ml of each respective solvent or solution, which was added to the same glass tubes used for synthesizing the material. The tubes were then sealed with polybutylene terephthalate caps containing a PTFE seal and were subsequently stirred and heated to various temperatures (as indicated in the 'Synthesis, structure and characterization of SU-102' section) for 24 h. Solutions of various pH were prepared by adding NaOH or HCl to deionized water to obtain the desired pH.

For ion exchange, 300 mg of the as-synthesized MOF was mixed with 100 ml 1 M solution of a metal chloride salt (LiCl, NaCl or KCl) for 30 min at room temperature. After 30 min, the partially ion-exchanged MOF was separated by centrifugation at 2,349*g* for 10 min and the process was repeated again for a second time. Thereafter, the ion-exchanged MOF was separated by centrifugation at 2,349*g* for 10 min and washed three times with 50 ml deionized water. After washing, the ion-exchanged MOF was dried in an oven at 343 K overnight.

For general characterization, in-house PXRD measurements were carried out using a Panalytical X'pert Pro diffractometer (Cu $K\alpha_{1,2}$, $\lambda_1 = 1.540598$ Å, $\lambda_2 = 1.544426$ Å) using a Bragg–Brentano geometry. Variable-temperature PXRD measurements were carried out using the aforementioned in-house diffractometer, equipped with an Anton Paar XRK 900 chamber (Supplementary Fig. 23). Thermogravimetric analysis (TGA) data (Supplementary Fig. 7) of as-synthesized SU-102 were collected using a PerkinElmer TGA 7. Secondary electron scanning electron microscopy images were acquired using a JEOL 7000F microscope operating at 2 kV (unless indicated otherwise in the Supplementary Information). Elemental analysis was carried out by Medac Ltd. The elemental analysis of as-synthesized SU-102 was as follows: expected (%) for $DMA_2[Zr(C_{14}H_3O_8)_2]{\cdot}6H_2O$: C 42.34, H 4.00, N 3.09; measured (%): C 47.28, H 4.12, N 2.81. The elemental analysis of activated SU-102 was as follows: expected (%) for $DMA_2[Zr(C_{14}H_3O_8)_2]$: C 47.46, H 2.74, N 6.92; measured (%): C 46.91, H 3.94, N 2.78.

Ultraviolet–visible (UV–vis) spectra (Supplementary Figs. 29–32) were acquired in diffuse reflectance mode with a PerkinElmer Lambda 1050 UV–vis–NIR spectrometer equipped with an integrating sphere, using $BaSO_4$ as the reflectance reference. The Kubelka–Munk function $F(RN) = k/s$ (where k and s are the absorption and diffusion coefficients, respectively) was applied to the data to obtain the corresponding absorbance spectrum.

3D electron diffraction and topological analysis

Three-dimensional electron diffraction data (Supplementary Fig. 5 and Supplementary Table 2) were collected using a JEOL JEM2100 TEM, equipped with a Timepix detector from Amsterdam Scientific Instruments, while continuously rotating the crystal at 0.45° s^{-1}. The experiment was carried out using Instamatic[37], with data reduction performed in XDS[38]. The acquired intensities were then used to solve the structure of SU-102 with SHELXT[39], and refined using SHELXL[40], with electron scattering factors extracted from SIR2014 (ref. 41). From the 3D ED data, all non-hydrogen atoms could be located in the initial structure solution. Hydrogen atoms were located in the difference Fourier maps of subsequent refinements. The phase purity of the title material was shown through a Pawley fit (Supplementary Fig. 3 and Supplementary Table 1) against PXRD data in TOPAS-Academic version 6 (ref. 42). Topological analysis of the SU-102 framework was carried out using the software package ToposPro[43].

STEM

Sample preparation for STEM imaging was performed by taking a small amount (~20 µg) of as-synthesized SU-102 and embedding it in a resin (LR White) inside a gelatin capsule (size 00). The capsule was then hardened at 60 °C for 24 h. Ultrathin sectioning, with an estimated section thickness of 40 nm, was later carried out using a Leica Ultracut UCT with a 45° diamond knife from Diatome. The sections were then transferred to carbon-coated copper grids (EMS-CF150-Cu-UL). STEM images of SU-102 were obtained using a Thermo Fisher Themis Z double aberration-corrected TEM. The microscope was operated at an accelerating voltage of 300 kV. The images were acquired using a beam current of 10 pA, a convergence angle of 16 mrad and a dwell time of 5 µs. iDPC and ADF images were obtained simultaneously. The ADF detector was set at a collection angle of 25–153 mrad. The iDPC images were formed using a segmented annular detector. A high-pass filter was applied to the iDPC images to reduce low-frequency contrast. The lattice-averaged potential maps were obtained by crystallographic image processing using the software CRISP[44].

Gas sorption

Nitrogen and greenhouse gas (CO_2 and SF_6) sorption measurements (Supplementary Figs. 11–18 and Supplementary Table 4) were carried out using a Micromeritics ASAP2020 surface area analyser. The analysis bath was temperature controlled using liquid nitrogen (194 K) or water (293 K). Gas selectivity was estimated using the equation $s_{gas1} = (q_{gas1}/q_{gas2})/(p_{gas1}/p_{gas2})$ for two hypothetical gases with 15 kPa CO_2: 85 kPa N_2 and 10 kPa SF_6: 80 kPa N_2. Before gas sorption measurements, the as-synthesized MOF was activated at 150 °C for 3 h under dynamic vacuum and the ion-exchanged MOFs were activated at 110 °C for 3 h under dynamic vacuum.

SO_2 adsorption in SU-102

The adsorption–desorption SO_2 isotherm was performed on an activated sample of SU-102, at 298 K up to 1 bar, with the aid of a dynamic gravimetric gas/vapour sorption analyser, DVS vacuum (Surface Measurement Systems Ltd.). The resulting adsorption isotherm is of type I with a total SO_2 uptake of 2.8 mmol g^{-1} (Supplementary Fig. 24). The PXRD pattern of SU-102 after SO_2 adsorption confirmed the retention of the crystal structure (Supplementary Fig. 25). Considering the relatively low surface area of SU-102, the SO_2 packing density within the pores is comparable to MOF materials with higher BET surface area such as NU-1000 and MFM-601, with a reported packing density of 0.65 and 0.53 g cm^3, respectively (see Supplementary Table 5 for a comparison). The heat of SO_2 adsorption in SU-102 was calculated according to reported literature[45]. Two SO_2 adsorption isotherms were measured at two different temperatures (Supplementary Fig. 26), and the isotherms in the low coverage region were fitted according to the virial-type equation (1), which expresses the pressure p as a function of the amount adsorbed n. A_0 is a virial coefficient for the adsorbate–adsorbent interaction, and A_1, A_2, etc. are constants for the double, triple and so on (A_2 and higher coefficents can be ignored at low coverage).

$$p = n \exp\left(\sum_{i=0}^{m} A_i n^i\right) \tag{1}$$

or in logarithmic form

$$\ln\left(\frac{n}{p}\right) = A_0 + A_1 n + A_2 n^2 + \ldots \tag{2}$$

A plot of $\ln(n/p)$ versus n should give a straight line at low surface coverage (Supplementary Fig. 27). Using the Clausius–Clapeyron equation (3), where Q_{st} is the heat of adsorption, T is temperature and R is the gas constant, for a fixed surface coverage n, equation (4) is obtained, where H_{ads} is the enthalpy of adsorption, and p_1 and p_2 are the partial pressures at temperatures T_1 and T_2, respectively. Substitution of p in equation (4) with equation (2) results in an expression for the enthalpy of adsorption (equation (5)). From the linear fittings, the virial coefficients are used to estimate the enthalpy of adsorption. The value obtained for the isosteric heat of adsorption at zero coverage is −45.31 kJ mol^{-1}.

$$\left(\frac{\partial \ln(p)}{\partial T}\right)_n = -\frac{Q_{st}}{RT^2}, \tag{3}$$

$$\ln\left(\frac{p_1}{p_2}\right) = -\frac{\Delta H_{ads}}{R}\left(\frac{1}{T_2} - \frac{1}{T_1}\right), \tag{4}$$

$$\Delta H_{ads} = -R\left[\left(A_0^{T_2} - A_0^{T_1}\right) + \left(A_1^{T_2} - A_1^{T_1}\right) n\right] \frac{T_1 T_2}{T_1 - T_2}. \tag{5}$$

Solid-state NMR spectroscopy measurements

MAS NMR experiments were performed at a magnetic field of 14.1 T (Larmor frequencies of 600.12, 150.92 and 158.74 MHz for ^1H, ^{13}C and ^{23}Na, respectively) on a Bruker Avance III spectrometer. All spectra were recorded with a 1.3 mm probe head and a 60 kHz MAS rate. Proton acquisitions involved a rotor-synchronized, double-adiabatic spin–echo sequence with a 90° excitation pulse of 1.25 µs followed by a pair of 50.0 µs tanh/tan short high-power adiabatic pulses with a 5 MHz frequency sweep[46,47]. All pulses operated at a nutation frequency of 200 kHz. A total of 512 signal transients with a 5 s relaxation delay were collected. The ^1H–^{13}C cross-polarization MAS experiments involved Hartmann–Hahn matched ^1H and ^{13}C radiofrequency fields applied for a 1.5 ms contact interval, SPINAL-64 ^1H decoupling and 131,072 scans collected using a 2 s relaxation delay. The ^1H and ^{13}C chemical shifts were referenced with respect to tetramethylsilane. The ^{23}Na acquisition involved a hard, 0.25 µs excitation pulse (100 kHz nutation frequency) and 4,096 scans collected using a 2 s relaxation delay. The ^{23}Na shift is reported with respect to solid NaCl at 7.21 ppm. See Supplementary Fig. 8 for the assignments of the observed shifts,

Adsorption and photodegradation of EOCs

The treatment of effluents from WWTPs using SU-102 was studied by mixing SU-102 or Na-exchanged SU-102 (1 mg ml^{-1} of effluent water) with effluent water acquired from IVL Swedish Environmental Research Institute's R&D facility in Hammarby Sjöstadsverk in Stockholm, Sweden. The treatment steps of the membrane bioreactor process in the plant consist of an activated sludge process and a final ultrafiltration. A 7 day composite sample was collected through pooling of daily flow-proportional samples, which was then used for the adsorption tests. After stirring activated SU-102 with the effluent water for 24 h, the mixture was filtered off (Pall 0.2 µm SUPOR Acrodisc filters) and analysed by HPLC–tandem mass spectrometry using solid phase extraction cartridges (Oasis HLB, 6 ml, Waters). Cartridges were conditioned with methanol followed by Milli-Q water. The substances were eluted from the solid phase extraction cartridges using 5 ml methanol followed by 5 ml acetone. The supernatants were transferred to vials for final analysis on a binary liquid chromatography system with auto injection (Shimadzu, Japan). The chromatographic separation was carried out using gradient elution on a C18 reversed-phase column (dimensions 50 × 3 mm^2, 2.5 µm particle size, XBridge, Waters) at a temperature of 35 °C and a flow rate of 0.3 ml min^{-1}. A procedural blank was also made and analysed. All the results are presented in Supplementary Tables 6 and 8.

For the laboratory-scale tests on solutions containing selected EOCs, the selected EOCs, At (≥98%), SMT (≥99%) and sodium DCF (≥98%) were purchased from Sigma-Aldrich and used without further purification. Different organic molecules were analysed by HPLC: the amount of adsorbed or degraded SMT, At and DCF as well as the released ellagic acid linker were determined using a reversed-phase HPLC Jasco LC-4000 series system, equipped with a photodiode array detector MD-4015 and a multisampler AS-4150 controlled by ChromNav software (Jasco Inc.). A purple octadecyl-silica reverse-phase column (5 µm, 4.6 × 150 mm, Análisis Vínicos) was employed. For the quantification of all chemical species, isocratic conditions were used. The flow rate was 1 ml min^{-1}, and the column temperature was fixed at 298 K. In all cases, the injection volume was 30 µl.

The mobile phase was based on a mixture of 70:20:10 water:acetronitrile:formic acid (10% vol/vol) solution for ellagic acid analysis, with a retention time (r.t.) and an absorption maximum of 5.99 min and 280 nm, respectively. SMT was analysed using a mixture of 35:65 acetonitrile:water, with a r.t. of 2.7 min and an absorption maximum of 263 nm. At was analysed using a mixture of 90:10 PBS:MeOH (PBS, 0.04 M, pH 2.5) with a r.t. of 4.81 min and an absorption maximum of 227 nm. DCF was analysed using a mixture of 70:30 acetonitrile:formic acid (10% vol/vol) solution with a r.t. of 3.75 min and an absorption maximum of 275 nm. To prepare the PBS (0.04 M, pH 2.5), 0.02 mol (2.4 g) NaH_2PO_4 and 0.02 mol (2.84 g) Na_2HPO_4 were dissolved in 1 l Milli-Q water. The pH was then adjusted to 2.5 with H_3PO_4 (≥85%).

In an 8 ml vial, 4 mg of SU-102 was suspended in 4 ml of a SMT, At or DCF aqueous solution made from tap water. The concentrations used were 10 mg l^{-1} for SMT, 70 mg l^{-1} for At and 15 mg l^{-1} for DCF. Adsorption or photodegradation reactions were performed under magnetic stirring in the dark (adsorption) or irradiating with visible light (photodegradation). At certain intervals (0.25, 0.5, 1, 2, 4, 5 and 24 h), an aliquot of 100 µl was collected by centrifugation for analysis by HPLC. In particular, the photodegradation studies were performed in a glass photoreactor equipped with a 300 W Xe lamp (Oriel Instruments OPS-A500) under open air at room temperature, with the samples stirred and placed at a fixed distance of 21 cm from the source. A 420 nm cut-off filter (Newport 20CGA-420 IJ342) was placed between the sample and the light source to eliminate the UV irradiation. It must be pointed out that before irradiation, it is not necessary to stir the suspension until the adsorption–desorption equilibrium is reached. All experiments were performed at least in triplicate to ensure statistically reliable results. The crystallinity of all the remaining solids was analysed by PXRD using an Empyrean diffractometer (PANalytical), equipped with a PIXcel3D detector and a Cu Kα radiation source (Ni β filter, $\lambda = 1.5406$ Å), operating at 45 kV and 40 mA. The liquid phases were analysed by HPLC, determining the amount of EOC and the total amount of possibly leached MOF ligand in the solution (see the HPLC conditions described above). Note here that the stability of SMT, At and DCF was studied under irradiation in the absence of the MOF, confirming that none of them were degraded after 24 h. The same procedure was used for studying the photodegradation of a mixture of the three selected EOCs (At, SMT and DCF), in which 4 mg of SU-102 was suspended in 4 ml of a mixture of At (70 mg l^{-1}), SMT (10 mg l^{-1}) and DCF (15 mg l^{-1}) in tap water. The mixture was then irradiated under visible light and continuous stirring. Aliquots of 100 µl were taken at different time intervals (0.25, 0.5, 1, 2, 4, 5, 6, 7 and 24 h) and centrifuged for HPLC analysis.

The degradation mechanism of SMT was determined by HPLC–MS using an Agilent 1260 Infinity II (Agilent Technologies). The system was coupled to a single quadrupole mass spectrometer detector (InfinityLab LC/MSD-iQ, Agilent Technologies), equipped with an atmospheric pressure ionization electrospray source, working in positive and negative ion mode and analysing samples in the mass range of 40–400 *m/z*. For the quantification of SMT, the mobile phase consisted of a mixture of acetonitrile:water (35:65) delivered at a flow rate of 0.5 ml min^{-1} at 35 °C and using a InfinityLab Poroshell 120 EC-C18 (2.1 × 150 mm; 2.7 µm) (Agilent Technologies) column.

The toxicity of the degradation products was assessed using quantitative structure–activity relationship calculations by the Toxicity Software Tool developed by the Environmental Protection Agency. The developmental toxicity was evaluated on the main degradation compounds (maleic acid, acetic acid and phenol) by applying the consensus method[48].

For regeneration of the adsorbent, desorption experiments using SU-102 loaded with At were performed using a saturated solution of NaCl. First, At was adsorbed into the MOF using a highly concentrated At solution in tap water of 1,000 ppm for a duration of 5 h. The MOF was then separated by filtration using a nylon filter (0.22 µm) under vacuum. The At loading was calculated by HPLC, reaching 0.20 ± 0.03 mg_{At} per $mg_{SU\text{-}102}$. The resulting At-loaded MOF was dispersed in a saturated solution of NaCl under continuous stirring at 400 r.p.m. An aliquot of 100 µl was taken at different time intervals. The results (Supplementary Fig. 34) showed that, after 15 min, the At release was 0.20 ± 0.01 mg_{At} per $mg_{SU\text{-}102}$ (corresponding to ~100% desorption of the previously loaded At), indicating complete regeneration of the SU-102 material.

Data availability

CCDC 2167934 contains the supplementary crystallographic data for this paper. These data can be obtained free of charge via www.ccdc.cam.ac.uk/data_request/cif, by emailing data_request@ccdc.cam.ac.uk, or by contacting The Cambridge Crystallographic Data Centre, 12 Union Road, Cambridge CB2 1EZ, UK (fax +44 1223 336033). Part of the raw data have been made available on Zenodo (record 7687564) (ref. 49).

References

1. Vörösmarty, C. J. et al. Global threats to human water security and river biodiversity. *Nature* **467**, 555–561 (2010).
2. Falkenmark, M., Wang-Erlandsson, L. & Rockström, J. Understanding of water resilience in the Anthropocene. *J. Hydrol. X* **2**, 100009 (2019).
3. Deblonde, T., Cossu-Leguille, C. & Hartemann, P. Emerging pollutants in wastewater: a review of the literature. *Int. J. Hyg. Environ. Health* **214**, 442–448 (2011).
4. Geissen, V. et al. Emerging pollutants in the environment: a challenge for water resource management. *Int. Soil Water Conserv. Res.* **3**, 57–65 (2015).
5. Yang, Y., Ok, Y. S., Kim, K. H., Kwon, E. E. & Tsang, Y. F. Occurrences and removal of pharmaceuticals and personal care products (PPCPs) in drinking water and water/sewage treatment plants: a review. *Sci. Total Environ.* **596–597**, 303–320 (2017).
6. Wilkinson, J. L. et al. Pharmaceutical pollution of the world's rivers. *Proc. Natl Acad. Sci. USA* **119**, 1–10 (2022).
7. Rojas, S. & Horcajada, P. Metal–organic frameworks for the removal of emerging organic contaminants in water. *Chem. Rev.* **120**, 8378–8415 (2020).
8. Landete, J. M. Ellagitannins, ellagic acid and their derived metabolites: a review about source, metabolism, functions and health. *Food Res. Int.* **44**, 1150–1160 (2011).
9. Arbenz, A. & Avérous, L. Chemical modification of tannins to elaborate aromatic biobased macromolecular architectures. *Green Chem.* **17**, 2626–2646 (2015).
10. Svensson Grape, E. et al. A robust and biocompatible bismuth ellagate MOF synthesized under green ambient conditions. *J. Am. Chem. Soc.* **142**, 16795–16804 (2020).
11. Piątek, J. et al. Toward sustainable Li-ion battery recycling: green metal-organic framework as a molecular sieve for the selective separation of cobalt and nickel. *ACS Sustain. Chem. Eng.* **9**, 9770–9778 (2021).
12. Chen, Z. et al. Reticular chemistry in the rational synthesis of functional zirconium cluster-based MOFs. *Coord. Chem. Rev.* **386**, 32–49 (2019).
13. Mouchaham, G. et al. A robust infinite zirconium phenolate building unit to enhance the chemical stability of Zr MOFs. *Angew. Chem. Int. Ed.* **54**, 13297–13301 (2015).
14. Mouchaham, G. et al. Adaptability of the metal(III,IV) 1,2,3-trioxobenzene rod secondary building unit for the production of chemically stable and catalytically active MOFs. *Chem. Commun.* **53**, 7661–7664 (2017).
15. Chen, E. X. et al. Acid and base resistant zirconium polyphenolate-metalloporphyrin scaffolds for efficient CO_2 photoreduction. *Adv. Mater.* **30**, 1–8 (2018).
16. Feng, X. et al. Elucidating J-aggregation effect in boosting singlet-oxygen evolution using zirconium-porphyrin frameworks: a comprehensive structural, catalytic, and spectroscopic study. *ACS Appl. Mater. Interfaces* **11**, 45118–45125 (2019).
17. Huang, Z., Grape, E. S., Li, J., Inge, A. K. & Zou, X. 3D electron diffraction as an important technique for structure elucidation of metal-organic frameworks and covalent organic frameworks. *Coord. Chem. Rev.* **427**, 213583 (2021).
18. O'Keeffe, M., Peskov, M. A., Ramsden, S. J. & Yaghi, O. M. The Reticular Chemistry Structure Resource (RCSR) database of, and symbols for, crystal nets. *Acc. Chem. Res.* **41**, 1782–1789 (2008).
19. Ebele, A. J., Abou-Elwafa Abdallah, M. & Harrad, S. Pharmaceuticals and personal care products (PPCPs) in the freshwater aquatic environment. *Emerg. Contam.* **3**, 1–16 (2017).

20. Neurath, G. B., Dünger, M., Pein, F. G., Ambrosius, D. & Schreiber, O. Primary and secondary amines in the human environment. *Food Cosmet. Toxicol.* **15**, 275–282 (1977).
21. Cheung, O. & Hedin, N. Zeolites and related sorbents with narrow pores for CO_2 separation from flue gas. *RSC Adv.* **4**, 14480–14494 (2014).
22. Cheung, O. et al. Highly selective uptake of carbon dioxide on the zeolite $|N_{a10.2}KCs_{0.8}|$-LTA—a possible sorbent for biogas upgrading. *Phys. Chem. Chem. Phys.* **18**, 16080–16083 (2016).
23. Decoste, J. B. et al. Stability and degradation mechanisms of metal-organic frameworks containing the $Zr_6O_4(OH)_4$ secondary building unit. *J. Mater. Chem. A* **1**, 5642–5650 (2013).
24. Syvab, R. *Main Report—Pharmaceutical Capture, Syvab (Förstudie läkemedelsrening Syvab)* (Swedish Environmental Institute and Stockholm University), 2019).
25. Salgado, R. et al. Assessing the removal of pharmaceuticals and personal care products in a full-scale activated sludge plant. *Environ. Sci. Pollut. Res.* **19**, 1818–1827 (2012).
26. García-Galán, M. J., González Blanco, S., López Roldán, R., Díaz-Cruz, S. & Barceló, D. Ecotoxicity evaluation and removal of sulfonamides and their acetylated metabolites during conventional wastewater treatment. *Sci. Total Environ.* **437**, 403–412 (2012).
27. Anadón, A., Martínez-Larrañaga, M. R., Ares, I., Castellano, V. & Martínez, M. A. in *Reproductive and Developmental Toxicology* 2nd edn. (Ed Gupta, R. C.) Ch. 5, 68–98 (Academic Press, 2017).
28. Schwaiger, J., Ferling, H., Mallow, U., Wintermayr, H. & Negele, R. D. Toxic effects of the non-steroidal anti-inflammatory drug diclofenac. Part I: histopathological alterations and bioaccumulation in rainbow trout. *Aquat. Toxicol.* **68**, 141–150 (2004).
29. Wang, N. et al. Sulfonamide-resistant bacteria and their resistance genes in soils fertilized with manures from Jiangsu province, Southeastern China. *PLoS ONE* **9**, e112626 (2014).
30. Chow, L. K. M., Ghaly, T. M. & Gillings, M. R. A survey of sub-inhibitory concentrations of antibiotics in the environment. *J. Environ. Sci.* **99**, 21–27 (2021).
31. Fekadu, S., Alemayehu, E., Dewil, R. & Van der Bruggen, B. Pharmaceuticals in freshwater aquatic environments: a comparison of the African and European challenge. *Sci. Total Environ.* **654**, 324–337 (2019).
32. Quadra, G. R. et al. Temporal and spatial variability of micropollutants in a Brazilian urban river. *Arch. Environ. Contam. Toxicol.* **81**, 142–154 (2021).
33. Shamsudin, M. S., Azha, S. F. & Ismail, S. A review of diclofenac occurrences, toxicology, and potential adsorption of clay-based materials with surfactant modifier. *J. Environ. Chem. Eng.* **10**, 107541 (2022).
34. Colella, C. Ion exchange equilibria in zeolite minerals. *Miner. Depos.* **31**, 554–562 (1996).
35. Rojas, S. et al. Towards improving the capacity of UiO-66 for antibiotic elimination from contaminated water. *Faraday Discuss.* **231**, 356–370 (2021).
36. Feng, Y. et al. Red mud powders as low-cost and efficient catalysts for persulfate activation: pathways and reusability of mineralizing sulfadiazine. *Sep. Purif. Technol.* **167**, 136–145 (2016).
37. Cichocka, M. O., Ångström, J., Wang, B., Zou, X. & Smeets, S. High-throughput continuous rotation electron diffraction data acquisition via software automation. *J. Appl. Crystallogr.* **51**, 1652–1661 (2018).
38. Kabsch, W. XDS. *Acta Crystallogr. D* **66**, 125–132 (2010).
39. Sheldrick, G. M. SHELXT—integrated space-group and crystal-structure determination. *Acta Crystallogr. A* **71**, 3–8 (2015).
40. Sheldrick, G. M. A short history of SHELX. *Acta Crystallogr. A* **64**, 112–122 (2008).
41. Burla, M. C. et al. Crystal structure determination and refinement via SIR2014. *J. Appl. Crystallogr.* **48**, 306–309 (2015).
42. Coelho, A. TOPAS-Academic V6 (Coelho Software, 2016).
43. Blatov, V. A., Shevchenko, A. P. & Proserpio, D. M. Applied topological analysis of crystal structures with the program package ToposPro. *Cryst. Growth Des.* **14**, 3576–3586 (2014).
44. Hovmöller, S. CRISP: crystallographic image processing on a personal computer. *Ultramicroscopy* **41**, 121–135 (1992).
45. Nuhnen, A. & Janiak, C. A practical guide to calculate the isosteric heat/enthalpy of adsorption: via adsorption isotherms in metal–organic frameworks, MOFs. *Dalton Trans.* **49**, 10295–10307 (2020).
46. Hwang, T., Van Zijl, P. C. M. & Garwood, M. Fast broadband inversion by adiabatic pulses. *J. Magn. Reson.* **133**, 200–203 (1998).
47. Kervern, G., Pintacuda, G. & Emsley, L. Fast adiabatic pulses for solid-state NMR of paramagnetic systems. *Chem. Phys. Lett.* **435**, 157–162 (2007).
48. Khan, K., Benfenati, E. & Roy, K. Consensus QSAR modeling of toxicity of pharmaceuticals to different aquatic organisms: ranking and prioritization of the DrugBank database compounds. *Ecotoxicol. Environ. Saf.* **168**, 287–297 (2019).
49. Svensson Grape E., Chacón-García A. J., Willhammar T. Raw data associated with the zirconium ellagate material SU-102. *Zenodo* https://doi.org/10.5281/zenodo.7687564 (2023).

Acknowledgements

The authors thank G. Maurin for insightful discussions. The authors also acknowledge funding from the following organizations: the Swedish Foundation for Strategic Research (SSF) (E.S.G. and A.K.I.), the Knut and Alice Wallenberg Foundation, KAW 2016.0072 (A.K.I.), the Swedish Research Council, VR 2019-05465 (T.W. and M.N.) and VR 2020-04029 (O.C and M.Å.), the Swedish Research Council for Sustainable Development, FORMAS 2022-01270 (T.W.) and FORMAS 2018-00651 (O.C and M.Å.), the MOFSEIDON project, PID2019-104228RB-100, MCI/AEI/FEDER, UE (A.C., S.R., Y.P. and P.H.), the Madrid Community, Recruitment of Young Doctors 2017, Modality 2, 2017-T2/IND-5149 (S.R.) and the Spanish Juan de la Cierva Incorporación Fellowship, grant agreement no. IJC2019-038894-I (S.R.).

Author contributions

E.S.G. designed and synthesized SU-102, collected 3D ED data and determined the crystal structure, performed PXRD, Pawley fitting, scanning electron microscopy, energy-dispersive X-ray spectroscopy, TGA, topological analysis, stability tests in organic solvents and various pH, and adsorption of EOCs from WWTP effluent. A.J.C.-G., S.R. and Y.P. performed laboratory-scale EOC adsorption and photodegradation experiments. A.J. performed and managed NMR experiments. M.N. prepared and sectioned samples for STEM imaging. E.M.-A. performed SO_2 sorption experiments. A.E.G.F. synthesized SU-102 in the absence of DMF. M.P. performed the ion exchange and regeneration experiments. M.N.-F. collected and provided WWTP effluent. I.A.I. managed the SO_2 sorption experiments. O.C. and M.Å. performed ion exchange and characterization of the ion-exchanged samples including the N_2, CO_2 and SF_6 sorption experiments. C.B. managed the WWTP effluent analysis. T.W. performed STEM analysis and managed TEM experiments. P.H. managed EOC adsorption, photodegradation and UV–vis experiments. A.K.I. supervised and managed the project. All authors provided feedback and discussed the manuscript.

Funding

Open access funding provided by Stockholm University.

Competing interests
The authors declare no competing interests.

Additional information
Supplementary information The online version contains supplementary material available at https://doi.org/10.1038/s44221-023-00070-z.

Correspondence and requests for materials should be addressed to Tom Willhammar, Patricia Horcajada or A. Ken Inge.

Peer review information *Nature Water* thanks Yangyang Liu, Joseph Mondloch and the other, anonymous, reviewer(s) for their contribution to the peer review of this work.